



# Heinrich events show two-stage climate response in transient glacial simulations

Florian Andreas Ziemen<sup>1</sup>, Marie-Luise Kapsch<sup>1</sup>, Marlene Klockmann<sup>1</sup>, and Uwe Mikolajewicz<sup>1</sup>

<sup>1</sup>Max Planck Institute for Meteorology, Bundesstraße 53, 20146 Hamburg, Germany

Correspondence to: Florian A. Ziemen ([florian.ziemen@mpimet.mpg.de](mailto:florian.ziemen@mpimet.mpg.de))

**Abstract.** Heinrich events are among the dominant modes of glacial climate variability. During these events, massive iceberg armadas were released by the Laurentide Ice Sheet, sailed across the Atlantic, and caused large-scale climate changes. We study these events in a fully coupled complex ice sheet–climate model with synchronous coupling between ice sheets and oceans. The ice discharges occur as internal variability of the model with a recurrence period of 5 kyr, an event duration of 5 1–1.5 kyr, and a peak discharge rate of about 50 mSv, roughly consistent with reconstructions. The climate response shows a two-stage behavior, with freshwater release effects dominating the surge phase and ice-sheet elevation effects dominating in the post-surge phase. As a direct response to the freshwater discharge during the surge phase, the deepwater formation in the North Atlantic decreases and the North Atlantic deepwater cell weakens by 3.5 Sv. With the reduced oceanic heat transport, the surface temperatures across the North Atlantic decrease, and the associated reduction in evaporation causes a drying in 10 Europe. The ice discharge lowers the surface elevation in the Hudson Bay area and thus leads to increased precipitation and accelerated ice sheet regrowth in the post-surge phase. Furthermore, the jet stream widens to the north and becomes more zonal. This contributes to a weakening of the subpolar gyre, and a continued cooling over Europe even after the ice discharge. This two-stage behavior can explain previously contradicting model results and understandings of Heinrich Events.

## 1 Introduction

15 While the climate of the last millenia has been comparatively stable, proxy records from the last glacial show large-scale rapid climate fluctuations. The two most prominent of these are Dansgaard-Oeschger (Dansgaard et al., 1984) and Heinrich events (Heinrich, 1988). Both of them are associated with a reorganization of the North Atlantic Ocean circulation (see Clement and Peterson, 2008, for a review). Here we focus on Heinrich events. In these events, that fall into the Dansgaard-Oeschger cold periods (Bond et al., 1992), iceberg armadas spread detritus from the Hudson Strait area across the North Atlantic seafloor 20 and caused large-scale climate changes. During the last glacial, six Heinrich events occurred at 16 800, 24 000, 31 000, 38 000, 45 000, and 60 000 years before present (Hemming, 2004). Thus, these events are considered quasi-periodic with a recurrence period of about 7 000 years.

The periodic ice rafting during Heinrich events can be explained by buildup–collapse (*binge-purge*) cycles of the Laurentide Ice Sheet (MacAyeal, 1993). In the multi-millennial buildup phase, the ice sheet grows until it becomes unstable and then 25 surges into the ocean. As possible triggers, sea level, or cold air temperatures were suggested (Bond and Lotti, 1995). Calov



et al. (2002) were able to obtain Laurentide Ice Sheet oscillations in simulations with the three-dimensional ice sheet model SICOPOLIS. They furthermore showed that, the timing of these events could be phase-locked to a 1500 year cycle resembling the Dansgaard-Oeschger cycles by perturbing the ice sheet at the mouth of Hudson Strait. While Calov et al. (2002) published their findings, a decoupling of cooling surface and warming sub-surface temperatures prior to the Heinrich events was found in  
5 North Atlantic sediment cores and enhanced oceanic melt was suggested as trigger for the ice discharges (Moros et al., 2002). This mechanism was reproduced in the three-dimensional ice sheet model GRISLI, where the outflow of a continuously active Hudson Strait Ice Stream was modulated by an ice shelf repeatedly blocking the Labrador Sea (Álvarez-Solas et al., 2011).

In climate models, the effects of such discharge events are commonly studied in freshwater perturbation (*hosing*) experiments (e. g. Maier-Reimer and Mikolajewicz, 1989; Schiller et al., 1997; Stouffer et al., 2006; Kageyama et al., 2013). These  
10 experiments can generally explain the large-scale cooling and the drying in Eurasia that are commonly observed in proxies. So far, there has only been one study investigating Heinrich events in a fully coupled ice sheet – climate model. In this study, Roberts et al. (2014b) used a 1:100 year asynchronous coupling between the Atmosphere-Ocean General Circulation Model (AOGCM) FAMOUS and the ice sheet model GLIMMER. Thus, while a Heinrich event lasted 1000 to 2000 years in the ice sheet model, it only lasted 10-20 years for the climate model. In these simulations the topography was the most important  
15 factor for determining the climate response and outweighed the freshwater signal in the ocean. However, hosing experiments have shown that the ocean needs several decades to fully respond to a freshwater forcing (e. g. Stouffer et al., 2006; Otto-Bliesner and Brady, 2010). Thus, the asynchronous coupling, which shortened the discharge from 1-2 kyr to 10-20 years, likely suppressed part of the ocean response. Here, we present the first results from coupled ice sheet model (ISM) – atmosphere-ocean-vegetation general circulation model (AOVGCM) Heinrich event simulations with synchronous coupling between the  
20 ice sheets and the ocean. Thus the full response of the ocean circulation can unfold and we can study the different phases of the climate response.

We investigated the characteristic properties of Heinrich events in general. To obtain an archetypal event, we performed a composite analysis of four Heinrich events obtained from three transient experiments. We first describe the setup and the experiments, then detail on the two-stage structure we observe in the composite and finally discuss how this unifies the results  
25 of freshwater hosing experiments with those of Roberts et al. (2014b).

## 2 Model and setup

### 2.1 Model and coupling

The simulations were performed with a coarse resolution (T31/GR30) setup of the CMIP3 Max Planck Institute climate model ECHAM5/MPIOM/LPJ (Mikolajewicz et al., 2007b) coupled with a 20 km Northern Hemisphere setup of the modified Parallel  
30 Ice Sheet Model (mPISM) version 0.3 (Bueller and Brown, 2009; Winkelmann et al., 2011 for PISM). In this setup, the models are coupled bidirectionally without flux correction or other anomaly methods. mPISM and a similar setup are described in Ziemen et al. (2014). The main characteristics of the setup, and the differences to Ziemen et al. (2014) are outlined in the following.



In all simulations used for the analysis, a configuration was used where atmosphere and ocean are coupled with a periodic-synchronous 1:10 coupling (Voss and Sausen, 1996; Mikolajewicz et al., 2007a). This means that the atmosphere model is only run for one out of ten years. This reduces the computational expense drastically and speeds up the simulations by a factor of three (wallclock time). After each fully coupled year, the ocean is forced for nine years with atmospheric fields, that are  
5 obtained by cycling through the previous five fully coupled years. While this coupling introduces a lag of up to 50 years in the atmosphere-ocean system, the average lag of about 25 years is less than 10% of the 300-year averaging window used throughout most of the analysis. Furthermore, most of the changes in the ice sheets driving the atmosphere-ocean system occur on a longer time scale, so the lag can be neglected in the analysis. Parallel to the climate model, the ice sheet model is run for ten years, so ice sheets and ocean are on the same time scale. In the analysis of atmosphere and ocean fields, only the  
10 fully coupled years are used. These are also used to obtain the fields for forcing the ice sheet model. Thus, when we speak of a 300 year mean of the ocean 2D (3D) fields, actually only 30 years of data with a 10-year spacing are used. This should yield comparable results to the full data as long as there are no signals with periods of exact multiples of 10 years are involved (aliasing).

The surface mass balance is computed using downscaled precipitation and temperatures in a Positive Degree Day (PDD)  
15 scheme in the ice sheet model. Shelf basal melt is computed from ocean temperature and salinity using the three-equation model of Holland and Jenkins (1999). Ice sheet elevation, fresh water fluxes, and ice-ocean heat fluxes are fed back to the climate model. As in Ziemen et al. (2014), the temperature standard deviation for the PDD scheme is computed from the 6-hourly atmosphere model output. Extending this method, a minimum sub-monthly standard deviation of 4 K is prescribed. This prevents the standard deviation from falling too low in areas, where ECHAM5 simulates melt and limits the surface  
20 temperature to 0°C.

In contrast to Ziemen et al. (2014), iceberg calving and shelf basal melt are limited to grid cells that are connected to the open ocean at least via a channel with a minimum width of one grid cell and a minimum depth of 400 m. Such channels may be covered by a floating ice shelf. As another improvement over the setup of Ziemen et al. (2014), the river routing directions in the hydrology scheme are computed interactively to account for ice sheet changes and isostatic rebound. The direct ice  
25 discharge into the ocean is modeled as freshwater input with an associated negative heat input that turns the fresh water flux into an ice flux. If the ocean is at the freezing point, this leads to immediate sea ice formation. Under pre-industrial conditions, this parametrization already captures most of the climatic effects of Northern Hemisphere icebergs (Bügelmayer et al., 2015).

## 2.2 Experiments

We analyze a composite of four Heinrich events from three experiments (Fig. 1a, Tab. 1, Section 2.3 for details on the composite  
30 analysis). These are one long experiment (ExA in the following, see video supplement) starting at 42 kyr BP and two shorter experiments (ExB and ExC) starting at 23 kyr BP. From ExA, we discard the first 10 kyrs as final phase of the spin-up and obtain two events starting at 31 kyr BP (A1), and 25.7 kyr BP (A2). From ExB and ExC, we obtain two Heinrich events starting at 22.4 kyr BP: B1 and C1. Later Heinrich events show an interference of the deglaciation and are discarded. All experiments were forced with transient insolation and greenhouse gas concentrations from reconstructions (Berger, 1978; Spahni and Stocker,



2006a, b; Lüthi et al., 2008). The Antarctic Ice Sheet and the bedrock topography outside the ice sheet domain were prescribed based on the ICE-5G 21 ka topography (Peltier, 2004). The topography is corrected for a global uniform sea level change computed from the modeled ice volume. In ExA, and ExB, the dynamic river discharge scheme routes the Nile into the Red Sea during the glacial. In ExC this scheme is improved and the Nile always feeds into the Mediterranean. The technical differences between the three experiments are small enough to consider them as comparable.

The common spinup of all experiments began with a LGM steady state experiment (Ziemen et al., 2014) exhibiting a large spurious ice sheet over Siberia that connected to the Cordilleran part of the Laurentide Ice Sheet via Alaska. This ice sheet partly is an artifact of steady-state LGM simulations (Heinemann et al., 2014) and is common in coupled ice-climate modeling (e. g. Bauer and Ganopolski, 2017). Its growth can be reduced by modeling the effect of dust (Krinner et al., 2011). During the first phase of the spinup, the ice sheet was removed by setting the ice thickness between 90 °E and 140 °W to zero and relaxing the bedrock in this region. The model was then equilibrated with fixed surface mass balance forcing and constant removal of all ice between 90 °E and 140 °W for 5000 years. This yielded ice sheets with smooth margins that did not extent into Eastern Siberia or Alaska. ExA was started from this state by setting the time to 42 kyr BP and using transient orbital and greenhouse gas forcing. ExB and ExC were initialized at 23 kyr BP from an experiment that was started parallel to ExA and covered the time between 42 kyr BP and 23 kyr BP with 1:10 asynchronous coupling between the climate model and the ice sheet model. While the ice sheet in Siberia was removed in the first phase spin-up, in the following phase, it formed again (Fig. 2).

### 2.3 Composite analysis

We perform all further analysis on a composite of all four events. This creates an archetypal event that has the characteristics that are common to all events. To create the composite, we align the events on a common time scale. We base this alignment on the freshwater discharge at the mouth of Hudson Strait to extract the peak discharge phase. The duration of the start phase of the surge varies from event to event, so aligning for the same start time of the surge would smear out the peak discharge. However, the rising flank of the discharge signal is steep in all events (Fig. 1b), and closely precedes the peak discharge. Hence, all events are aligned so they cross 30 mSv Hudson Strait discharge in year 250, and the first surge (C1) starts in year 0. This leads to a relatively sharp peak in the discharge in years 300–600.

As the Heinrich events are part of the internal variability of the model, there is no control run without the effect of Heinrich events. Therefore, we use a composite of the 400 years (40 years in the atmosphere) before the events (here referred to as pre-surge phase) as reference state. We define two further time windows for the analysis: the surge phase (years 300–600), which covers the peak discharge, and the post-surge phase (years 1100–1400), which covers the minimal ice sheet volume at the end of the surge. During the surge phase, the climate is maximally affected by the freshwater discharge while the height of the ice sheet is slowly decreasing. In the post-surge phase, the ice discharge returns to its background level, while the ice sheet height loss peaks and its signal becomes dominant. As all averages are taken across the four events, they cover a total of 1600 years for the pre-surge phase, and 1200 years for the surge and post-surge phases.



ID	Experiment	Surge start composite year	Surge Start years BP	Surge End years BP	Duration years	Max flux mSv	Mean flux mSv
A1	ExA	110	31060	29610	1450	53	29
A2	ExA	70	25680	24350	1330	53	34
B1	ExB	35	22420	21270	1150	47	30
C1	ExC	0	22420	21560	860	55	28

**Table 1.** Events investigated. The surge start is defined by the surge branching off the Ungava Bay ice stream and propagating towards Hudson Bay. Its time is given in years BP and as the year in the composite. The end of the surge is defined as the time when there is no more surging in Hudson Strait. The maximum flux is defined as the maximum of 30-year running means, matching Fig. 1b.

### 3 Results

#### 3.1 The climate in the pre-surge phase

The climate in the pre-surge phase is a mean of different times before the Last Glacial Maximum (Tab. 1). Therefore, it is representative of the cold phase of the last glacial, but not specifically of the Last Glacial Maximum, which is used in most steady-state glacial climate studies. The global mean near-surface air temperature in the pre-surge phase is 3.2 K below the temperature in a pre-industrial experiment with the same model. The cooling is strongest over the ice sheets (Figs. 2–4). The North Atlantic Deepwater (NADW) is mainly formed south of Greenland and in the Nordic Seas (Fig. 5c, d). The NADW cell of the Atlantic Meridional Overturning Circulation (AMOC) has a maximum strength of 19 Sv at 30°N and reaches down to about 2900 m. For pre-industrial conditions, the modeled AMOC has the same depth and a strength of 15.8 Sv.

The Laurentide ice sheet is split into a Cordilleran and a Hudson Bay part (Fig. 4). The Hudson Bay part is connected to the Greenland Ice Sheet, which has grown to fill the entire Greenlandic shelf. Similarly, Iceland is covered in ice. The Fennoscandian Ice Sheet extends over large parts of Scandinavia as well as the Barents and Kara Sea shelves. In Eastern Siberia, a spurious ice sheet has formed (Section 2.2).

#### 3.2 The ice dynamics

A large part of the ice discharge into the ocean is channeled in ice streams. Some of them are constantly active (Fig. 2), while most of them, such as the Hudson Strait Ice Stream (24 in Fig. 2), perform surge cycles alternating between active and inactive states (see video supplement). The ice discharge at the mouth of Hudson Strait strongly varies (Fig. 1). When the Hudson Strait Ice Stream and the Ungava Bay Ice Stream (16 in Fig. 2) are quiescent, only 1 mSv of freshwater is discharged. Much of the time, the Ungava Bay Ice stream delivers about 5 mSv. At intervals of about 5 000 years, the Hudson Strait Ice Stream surges for a period of about 1000–1500 years with a peak discharge of about 50 mSv (Fig. 1).

All surges start with low discharge rates, while the surge is propagating inland in Hudson Strait (Figs. 1, 2). Between years 150 and 250 of the composite, the surges in all events reach Hudson Bay (not shown). This causes the steep increase in the



discharge signal, that we use to align the events. Around year 450 the northern part of Hudson Bay is surging in all four events. The exact shape of the surging area varies between the experiments. In A2 and B1 a second pulse in the discharge results from a delayed propagation of the surge the into southern part of Hudson Bay. In A1, this region is reached in the early stage of the surge. As the propagation of the surge varies from event to event, so does the duration with surge termination in C1 after 860  
5 years and in A1 after 1450 years (Table 1). The surge drains ice from the Hudson Bay area and the surface elevation decreases by up to 900 m (Fig. 4). The strongest decrease in surface elevation is located in Hudson Strait. The losses tail off towards the interior of Hudson Bay. The eastern part of the Laurentide Ice Sheet reaches its minimum volume around year 1200 of the composite. The ice loss of 0.8 Mio Gt, from 16.2 Mio Gt (year 50) to 15.4 Mio Gt (year 1200), corresponds to a sea level rise of about 2.3 m. This is followed by a slow recovery of the ice sheet, which takes more than 3000 years (Fig. 1). All other ice  
10 sheets show no significant deviations from the background behavior with growth of the Eastern Siberian Ice sheet in ExA and onset of the deglaciation in the late recovery phases of events B1 and C1.

### 3.3 The ocean response

Our coupling scheme represents iceberg calving and sub-shelf melt as a freshwater flux with an associated negative latent heat flux to the ocean. Thus, when the ice from the Hudson Strait Ice Stream enters the ocean, sea ice forms in the ocean model.  
15 During the surge phase (years 300–600), most of the additional sea ice follows the Labrador Current out of the Labrador Sea and melts in the open North Atlantic (Fig. 6a). On its way, the sea ice shields the ocean from the atmosphere and thus contributes to a reduction in ocean heat release (Fig. 8), especially in winter, when the decrease in heat release reaches  $70 \text{ W m}^{-2}$  in parts of the Labrador Basin (not shown) and the near surface air temperature decreases by up to 4 K (Fig. 5e for the annual mean). In summer, the increased sea-ice cover increases the albedo and reduces the net shortwave absorption with a maximum decrease  
20 of  $20 \text{ W m}^{-2}$  at the mouth of Hudson Strait (not shown). When the sea ice melts, the surface water freshens (Fig. 5a) and the stratification stabilizes (see below). In the post-surge phase (years 1100–1400), the sea-ice concentration in the Labrador Sea partially returns to pre-surge levels. In the Irminger Basin, the sea-ice margin advances, and the sea-ice cover in the Nordic Seas grows (Fig. 6a). The increased ice cover matches with a weaker subpolar gyre (see below; Fig. 7a) and a following slight expansion of the East Greenland Current indicated by a cooling and freshening at the eastern Margin of the current (Fig. 5b, d).  
25 In the Nordic Seas, the additional sea ice reduces the winter ocean heat release by up to  $50 \text{ W m}^{-2}$  (not shown), exceeding the regional reductions during the surge-phase.

During the surge phase, the freshwater released from the melting ice takes a strongly zonal path, and spreads across the whole Atlantic between  $40^\circ\text{N}$  and  $50^\circ\text{N}$  (Fig. 5a). Most of it passes south of the deep water formation areas (Fig. 5a; Fig. 5c for the pre-surge phase mixed layer depth). Still, some of it reaches the deep water formation areas, and the SSS in the areas  
30 with a time maximum winter mixed layer depth of more than 1000 m decreases by  $0.35 \text{ g kg}^{-1}$ . The convection depth in all deep water formation areas is reduced (Fig. 5a, c) and the 300 year running mean of the maximum winter mixed layer volume in the Atlantic north of  $40^\circ\text{N}$ , the Nordic Seas and the Arctic Ocean shrinks from  $6.4 \text{ Mio km}^3$  in the pre-surge phase to  $4.7 \text{ Mio km}^3$  ( $-27\%$ ) during the surge phase. As a result, the NADW cell weakens from  $18.3 \text{ Sv}$  to  $14.8 \text{ Sv}$  ( $-19\%$ ) in the same period (Fig. 8). The Arctic Ocean SSS also decreases (Fig. 5a). This is mostly due to a  $4 \text{ mSv}$  surge of the Amundsen Gulf Ice



Stream (18 in Fig. 2), 10% of the Hudson Strait flux. The freshening in the Arctic Ocean is limited by the halocline depth (not shown), so the total volume affected is much smaller than in the case of the Hudson Strait surge. In the post-surge phase, the sea-surface salinity in the North Atlantic largely recovers, but remains below its pre-surge levels. The SSS in the deep water formation areas remains about  $0.25 \text{ g kg}^{-1}$  below pre-surge levels. It reaches the pre-surge values after year 1500, when the mixed layer volume also recovers (not shown). The winter mixed layer depth in the central North Atlantic and the Nordic Seas remains decreased, while it recovers off the coasts of Ireland and Scotland (Fig. 5b, d). The still reduced mixed layer depth could be the reason why the salinity remains decreased even after the termination of the surge. Less deep mixing can be caused by a freshwater lid, on the other hand, it also means that less mid-depth high salinity water is brought to the surface. The NADW cell has mostly recovered (Fig. 8b).

The increase in sea-ice cover and the reduction in the deep water formation caused by the ice discharge during the surge phase lead to lower sea surface temperatures in the North Atlantic (Fig. 5c). In the Labrador Sea, and along the sea-ice margin, this cooling can be at least partly attributed to the increased sea-ice cover (Fig. 6a). The cooling is strongest in the open North Atlantic. With the slowdown of the meridional overturning circulation (Fig. 8b) less heat is brought into the subpolar gyre and the entire water column cools (not shown) and the heat release to the atmosphere is reduced on a large scale (Fig. 8c for the time series). In the post-surge phase, the meridional overturning circulation and the sea-surface temperatures largely recover. The remaining cooling signal is strongest at the sea ice margin (Figs. 5d, 6b). Along the margin between subtropical and subpolar gyre, a slight northward shift of the gyre front leads to a surface warming (Fig. 5d) that contrasts with generally cool sea surface temperatures. This warming is more expressed at intermediate depth and reaches down to 1500 m (not shown).

During the surge phase, the fresh water released from the melting ice is drawn down in the deep water formation areas and follows the NADW cell. Because of the NADW's reduced density, the Atlantic Antarctic Bottom Water (AABW) cell can expand slightly, decreasing the temperatures in the transition zone between NADW and AABW at a depth of about 3 km (not shown). The Atlantic subpolar gyre strengthens and reaches up to 55 Sv. This strengthening occurs despite a reduced wind driven component (Fig. 7). It is caused by an increase in the cross-gyre density gradient (not shown). The convection brings fresher, but also colder water down in the core of the subpolar gyre. The temperature effect in the core partially offsets the salinity effect. At the same time, the margins of the gyre freshen without significant temperature change, and the density contrast between core and margins of the gyre grows. In the post-surge phase, temperature and salinity begin to recover. The in-situ density in the core of the gyre remains reduced, while it recovers faster in the margins. In combination with a still reduced wind driven component, this weakens the gyre to 42 Sv. The gyre reaches its pre-surge strength around year 1500, with strong multi-centennial variability that matches the wind stress forcing (Fig. 7).

### 3.4 The atmosphere response

Heinrich events affect the atmosphere in two ways, here called the direct and the indirect effect. During the surge-phase, the indirect effect via freshwater-release induced changes in sea-ice concentration, and ocean heat transport and release (see above, Fig. 8c) dominates. In the post-surge phase, the freshwater release ceases, and the direct effect takes over: The decreasing ice sheet height (Fig. 4, overlays in 5e,f) directly influences the large-scale circulation. This effect already appears in the surge



phase and is strengthened in the post-surge phase. It leads to a northward shift of the jet stream over the west Atlantic (Fig. 9). Further, the jet stream becomes more zonal. The zonalization brings cold air into Europe (Fig. 5) and reduces the wind-driven transport in the Atlantic subpolar gyre (see above, Fig. 7).

During the surge phase, reductions in near-surface air temperatures (Fig. 5e) can be observed along the path of the sea-ice out of the Hudson bay, and over the southern part of the subpolar gyre, where the decreases in sea surface temperature are largest. The reduced ocean heat release (Fig. 8c) shows that the ocean is causing this cooling, which then is spread across the high latitudes by the winds. Due to the smaller ice sheet, the temperatures in the Hudson Bay area rise (see below). In the post-surge phase (Fig. 5f), the cooling is strongest along the sea-ice margin (Fig. 6b), where the sea-surface temperature changes are amplified by the effects of the increased ice cover. In these areas the ocean heat loss still is reduced, while over the open North Atlantic the picture is less clear with areas of increased and decreased ocean heat release. Here the effects of the zonalization of the jet stream and the changes in ocean circulation intermingle. The warming over the Hudson bay is strengthened (see below).

Due to the reduced ocean heat transport and the consequential cooling of the North Atlantic sector during the surge phase, (Fig. 5c–f), the evaporation decreases by 10% (North Atlantic and all connected basins north of 45°N, not shown). Over Europe, this results in a decrease in precipitation by 4–5% (Figs. 10b, 11c) that spreads far into Siberia. A northwest-southeast dipole pattern in the precipitation over the tropical Atlantic indicates a southeastward shift of the ITCZ. This pattern extends into Africa, with a southward shift of the tropical rain belt leading to a dipole pattern with drying in the Sahel Zone and an increase in the precipitation over southern Africa. In the post-surge phase, the evaporation over the North Atlantic partially recovers (not shown) and so does the precipitation in Europe (Fig. 10c, 11d). A slight large-scale reduction in evaporation remains in the tropical Atlantic, and the Sahel region (not shown). The dipole precipitation pattern in the Atlantic ITCZ turns into a monopole with a slight precipitation increase (Fig. 10c). The dipole pattern over Africa is slightly weakened but remains intact.

In the Hudson Bay area, the surface air temperature rises throughout the surge. This is in part due to the lapse-rate effect of the reduced surface elevation resulting from the surge. However, a closer look reveals that in both, the surge phase and the post-surge phase, the warming is more zonal and centered further to the south than expected from the lapse-rate effect alone (Fig. 5e, f). In the following, we describe the changes in the Hudson Bay area during the post-surge phase, as the basic behavior during the surge-phase is identical, just with a lower amplitude. We find an increase in total heat transport convergence in the southern Hudson Bay area by about  $3 \text{ W m}^{-2}$  (not shown). The eastern half of the area of depression experiences an increase in cloud cover (Fig. 11a, b). It is associated with an increase in surface net longwave radiation by  $5\text{--}6 \text{ W m}^{-2}$ , while the net shortwave radiation remains constant (not shown). The increase in cloud cover brings an increase in precipitation, locally reaching  $50 \text{ mm yr}^{-1}$  (+50%) (Fig. 11). The increased precipitation decreases the mass loss of the ice sheet during the surge and accelerates its regrowth.



#### 4 Discussion

The surges in our ice sheet model are based on an internal oscillation of the ice sheet, as described analytically by MacAyeal (1993) and first modeled in a three-dimensional ice sheet model by Calov et al. (2002). While the occurrence and properties of these oscillations are highly model-dependent (Calov et al., 2010), they are a robust feature of our ice sheet model in coupled  
5 as well as stand-alone setups (not shown) and have also been observed by other groups using PISM (Van Pelt and Oerlemans, 2012; Feldmann and Levermann, 2017). For modeling surges in our model with the Shallow Shelf Equation stress balance controlling the sliding, a horizontal resolution that properly resolves Hudson Strait proved necessary. In our simulations, the Hudson Strait Ice Stream was constantly active at 40 km model resolution (not shown); doubling the resolution to 20 km yielded the surge cycles.

10 The surge intensity and period are model dependent and affected by the surface temperature, the surface mass balance, as well as by the basal friction law (Calov et al., 2010). The slightly too short period in our model of 5 kyr instead of the 7 kyr derived from proxy records can be due to any combination of these factors. Since this kind of experiment takes a very long time on the supercomputer, we could not fine-tune the surge interval. However, the peak discharge rate of about 50 mSv agrees with the result obtained by Roberts et al. (2014a, b, 2016). Our surges with a duration of –1.5 kyr are shorter than the 3 kyr surges  
15 in their experiments, and with a cycle duration of 5 kyr, they are more frequent compared to 11 kyr cycles in their experiments. The surges in our study show an average loss of 0.96 Mio km<sup>3</sup> of ice, as compared to 2.5 Mio km<sup>3</sup> in their experiments.

Jongma et al. (2013) model HE1 as a 300 year 0.235 Sv discharge under LGM conditions. When including iceberg freshwater and latent heat fluxes, they simulate the strongest surface freshening in the frontal zone of the Newfoundland Basin, with a strong decrease of the freshening towards the east. They show that the feedback of the latent heat flux from iceberg melt on  
20 the ocean drastically reduces the iceberg melt in the Labrador sea as compared to modeling the freshwater flux only, and that it leads to an increased formation of sea ice. By modeling the calving as sea ice, we over-represent this effect. The melt is much more concentrated on the sea-ice edge, as the sea ice is not able to cross the open North Atlantic. All in all, the surface freshening is more zonal during the main discharge phase in our experiments than in Jongma et al. (2013). The icebergs in their model are not strictly tied to the ocean circulation and can more easily cross gyre fronts. This allows for a wider spread of the  
25 freshwater signal.

The comparison to climate proxy reconstructions is somewhat complicated, as Heinrich events generally fall into the Dansgaard-Oeschger stadials which are missing in our model. Climate proxies, therefore contain a combined signal of the stadial and the Heinrich events. While most Heinrich event studies focus on HE1, which fell into the deglaciation and is associated with a collapse of the AMOC (Stanford et al., 2011, e. g.), Lynch-Stieglitz et al. (2014) showed that there was little  
30 change of the Gulf Stream in the Florida Strait during HE2 and HE3, which fall into the same period as the events we study. Nonetheless, we can compare our results to the main features found in climate proxy reconstructions and single-forcing climate model experiments.

During the surge phase, the freshwater discharge is the dominant forcing in our model. This can be seen from the timing of the strong cooling and reduction in ocean heat release over the North Atlantic that strictly follows the freshwater input and SSS



changes (Figs. 1, 5, 8). The large-scale cooling, the decrease in NADW formation, and the southeastward shift of the ITCZ are consistent with proxy reconstructions (see the review of Clement and Peterson, 2008), as well as freshwater hosing experiments, where the surface elevation effect generally is not represented. In our experiments as well as in the freshwater hosing studies, the freshening reduces the Atlantic heat transport and thus causes a dipole anomaly in the sea surface temperatures with cooling in the North (Fig. 5c) and a slight warming in the South (not shown). This is generally associated with the southeast shift of the ITCZ (Stouffer et al., 2006, e. g.).

The decrease in the NADW cell strength by 19 % is on the weak end of freshwater hosing studies (Stouffer et al., 2006; Kageyama et al., 2013; Otto-Bliesner and Brady, 2010). This is of little surprise, as the freshwater perturbation from the surging ice sheet is weaker than the forcings prescribed in most of these studies, and the decrease of the NADW cell strength is highly correlated to the strength of the freshwater forcing (e. g. Maier-Reimer and Mikolajewicz, 1989; Stouffer et al., 2006). Furthermore, the modeled discharge into the Labrador sea allows a large fraction of the freshwater to escape into the subtropical gyre, while in most hosing experiments, the freshwater is spread more efficiently over the deepwater formation areas.

In the post-surge phase, we observe signals that are more consistent with the surface elevation effect described in Roberts et al. (2014b), where the ocean dynamics response was weakened by the 1:100 asynchronous coupling, and thus mostly the elevation signal remains. The jet stream becomes more zonal and the southward shift of the Atlantic ITCZ during the surge phase turns into a precipitation increase in the post-surge phase, when the topographic changes are largest. This two-phase behavior corresponds to two different experiments of Roberts et al. (2014b). They obtain the freshwater-related southward ITCZ shift only for a high freshwater release, while the experiment with pure topography changes shows the increase in precipitation that we obtain in the later phase.

Not all changes agree between our simulation and that of Roberts et al. (2014b). In our model, there is a west-east gradient in the precipitation change across Hudson Bay with increases on the eastern side (Figs. 10, 11). This contrasts with the results of Roberts et al. (2014b), where the precipitation over Hudson Bay decreases while the strongest increases are evident southeast of the bay. One factor contributing to such different behavior might be the different ice sheet shapes. We simulate a two-part Laurentide Ice Sheet, Roberts et al. (2014b) simulate one contiguous Laurentide Ice Sheet with the main dome in the southwest corner. As more coupled ice sheet–climate models are developed, further coupled studies will help distinguishing between model-specific and more robust effects.

## 5 Conclusions

By modeling Heinrich events as MacAyeal–style binge-purge cycles in a coupled ISM-AOVGCM system, we are able to observe a two-step response of the climate system: first to the freshwater discharge, and later to the elevation decrease over the Laurentide Ice Sheet. The freshwater discharge yields an increased stratification of the North Atlantic surface waters. The stronger stratification causes a reduction of deep water formation. This weakens the North Atlantic meridional overturning circulation and reduces the heat loss to the atmosphere. The colder conditions over the North Atlantic affects the North-South sea surface temperature gradient and thus shifts the Atlantic intertropical convergence zone southeastward. This behavior is



also known from freshwater hosing experiments. Furthermore, the cooling over the North Atlantic reduces the evaporation and thus precipitation in this region and downwind in Eurasia. In contrast to freshwater hosing experiments, we also see the effects of the reduced surface elevation on the atmospheric circulation. The surface elevation effects reach their maximum when the freshwater discharge ceases and the elevation of the Laurentide Ice Sheet is at its minimum. The lower elevation allows for a northward expansion and zonalization of the jet stream. This weakens the subpolar gyre and reduces the heat transport into (northern) Europe. Furthermore the lowered surface elevation allows for more precipitation over the Hudson Bay area and thus speeds up the regrowth of the Laurentide Ice Sheet.

Modeling ice sheets in fully coupled ISM-AOVCAM systems allows to study the full interactions between ice sheets and the climate. Only by modeling using an ice sheet model, we could obtain a physically plausible and self-consistent set of freshwater fluxes and ice sheet surface changes that led to the observed two-stage behavior, explaining the previous results from hosing experiments as well as elevation change experiments.

## 6 Data availability

The model output can be obtained from Florian Ziemen ([florian.ziemen@mpimet.mpg.de](mailto:florian.ziemen@mpimet.mpg.de)) upon request.

*Author contributions.* F. Z. and U. M. developed the setup. U. M. performed the experiments. F. Z. analyzed the data and wrote the manuscript. All authors discussed the analysis and manuscript.

*Competing interests.* U. M. is a member of the editorial board of the journal. The authors declare that they have no other conflicts of interest.

*Acknowledgements.* This work was supported by German Federal Ministry of Education and Research (BMBF) as Research for Sustainability initiative (FONA); through the project PalMod (FKZ: 01LP1502A). All simulations were performed at the German Climate Computing Center (DKRZ). The authors thank Thomas Kleinen for his comments which helped to improve the manuscript.



## References

- Álvarez-Solas, J., Montoya, M., Ritz, C., Ramstein, G., Charbit, S., Dumas, C., Nisancioglu, K., Dokken, T., and Ganopolski, A.: Heinrich event 1: an example of dynamical ice-sheet reaction to oceanic changes, *Clim. Past*, 7, 1297–1306, <https://doi.org/10.5194/cp-7-1297-2011>, <http://www.clim-past.net/7/1297/2011/>, 2011.
- 5 Bauer, E. and Ganopolski, A.: Comparison of surface mass balance of ice sheets simulated by positive-degree-day method and energy balance approach, *Climate of the Past*, 13, 819–832, <https://doi.org/10.5194/cp-13-819-2017>, <https://www.clim-past.net/13/819/2017/>, 2017.
- Berger, A. L.: Long-term variations of caloric insolation resulting from the earth's orbital elements, *Quat. Res.*, 9, 139–167, [https://doi.org/10.1016/0033-5894\(78\)90064-9](https://doi.org/10.1016/0033-5894(78)90064-9), <http://www.sciencedirect.com/science/article/pii/0033589478900649>, 1978.
- Bond, G., Heinrich, H., Broecker, W. S., Labeyrie, L., Mcmanus, J., Andrews, J., Huon, S., Jantschik, R., Clasen, S., Simet, C., Tedesco, K.,  
10 Klas, M., Bonani, G., and Ivy, S.: Evidence For Massive Discharges of Icebergs Into the North-atlantic Ocean During the Last Glacial Period, *Nature*, 360, 245–249, <http://dx.doi.org/10.1038/360245a0>, 1992.
- Bond, G. C. and Lotti, R.: Iceberg discharges into the north atlantic on millennial time scales during the last glaciation., *Science*, 267, 1005–10, <https://doi.org/10.1126/science.267.5200.1005>, <http://dx.doi.org/10.1126/science.267.5200.1005>, 1995.
- Bueler, E. and Brown, J.: Shallow shelf approximation as a sliding law in a thermomechanically coupled ice sheet model, *J. Geophys. Res.*,  
15 114, F03 008, <https://doi.org/10.1029/2008JF001179>, 2009.
- Bügelmayer, M., Roche, D. M., and Renssen, H.: How do icebergs affect the Greenland ice sheet under pre-industrial conditions? – a model study with a fully coupled ice-sheet–climate model, *Cryosph.*, 9, 821–835, <https://doi.org/10.5194/tc-9-821-2015>, <http://www.the-cryosphere.net/9/821/2015/>, 2015.
- Calov, R., Ganopolski, A., Petoukhov, V., Claussen, M., and Greve, R.: Large-scale instabilities of the Laurentide ice sheet simulated in a  
20 fully coupled climate-system model, *Geophys. Res. Lett.*, 29, 69–1—69–4, <https://doi.org/10.1029/2002GL016078>, 2002.
- Calov, R., Greve, R., Abe-Ouchi, A., Bueler, E., Huybrechts, P., Johnson, J. V., Pattyn, F., Pollard, D., Ritz, C., Saito, F., and Tarasov, L.: Results from the Ice-Sheet Model Intercomparison Project–Heinrich Event INtercOmparison (ISMIP HEINO), *J. Glaciol.*, 56, 371–383, <https://doi.org/10.3189/002214310792447789>, <http://openurl.ingenta.com/content/xref?genre=article&issn=0022-1430&volume=56&issue=197&spage=371>, 2010.
- 25 Clement, A. C. and Peterson, L. C.: Mechanisms of abrupt climate change of the last glacial period, *Rev. Geophys.*, 46, RG4002, <https://doi.org/10.1029/2006RG000204>, <http://dx.doi.org/10.1029/2006RG000204>, 2008.
- Dansgaard, W., Johnsen, S., Clausen, H., Dahl-Jensen, D., Gundestrup, N., Hammer, C., and Oeschger, H.: North Atlantic climatic oscillations revealed by deep Greenland ice cores, in: *Clim. Process. Clim. Sensit.*, vol. 29 of *Geophys. Monogr. Ser.*, pp. 288–298, AGU, Washington, DC, <https://doi.org/10.1029/GM029p0288>, <http://dx.doi.org/10.1029/GM029p0288>, 1984.
- 30 Feldmann, J. and Levermann, A.: From cyclic ice streaming to Heinrich-like events: the grow-and-surge instability in the Parallel Ice Sheet Model, *The Cryosphere*, 11, 1913–1932, <https://doi.org/10.5194/tc-11-1913-2017>, 2017.
- Heinemann, M., Timmermann, A., Elison Timm, O., Saito, F., and Abe-Ouchi, A.: Deglacial ice sheet meltdown: orbital pacemaking and CO<sub>2</sub> effects, *Clim. Past*, 10, 1567–1579, <https://doi.org/10.5194/cp-10-1567-2014>, 2014.
- Heinrich, H.: Origin and consequences of cyclic ice rafting in the Northeast Atlantic Ocean during the past 130,000 years, *Quat. Res.*, 29,  
35 142–152, [https://doi.org/10.1016/0033-5894\(88\)90057-9](https://doi.org/10.1016/0033-5894(88)90057-9), 1988.
- Hemming, S. R.: Heinrich events: Massive late Pleistocene detritus layers of the North Atlantic and their global climate imprint, *Rev. Geophys.*, 42, <https://doi.org/10.1029/2003RG000128>, 2004.



- Holland, D. M. and Jenkins, A.: Modeling Thermodynamic Ice–Ocean Interactions at the Base of an Ice Shelf, *J. Phys. Oceanogr.*, 29, 1787–1800, [https://doi.org/10.1175/1520-0485\(1999\)029<1787:MTIOIA>2.0.CO;2](https://doi.org/10.1175/1520-0485(1999)029<1787:MTIOIA>2.0.CO;2), 1999.
- Jongma, J. I., Renssen, H., and Roche, D. M.: Simulating Heinrich event 1 with interactive icebergs, *Clim. Dyn.*, 40, 1373–1385, <https://doi.org/10.1007/s00382-012-1421-1>, 2013.
- 5 Kageyama, M., Merkel, U., Otto-Bliesner, B., Prange, M., Abe-Ouchi, A., Lohmann, G., Ohgaito, R., Roche, D. M., Singarayer, J., Swingedouw, D., and X Zhang: Climatic impacts of fresh water hosing under Last Glacial Maximum conditions: a multi-model study, *Clim. Past*, 9, 935–953, <https://doi.org/10.5194/cp-9-935-2013>, 2013.
- Krinner, G., Diekmann, B., Colleoni, F., and Stauch, G.: Global, regional and local scale factors determining glaciation extent in Eastern Siberia over the last 140,000 years, *Quat. Sci. Rev.*, 30, 821–831, <https://doi.org/10.1016/j.quascirev.2011.01.001>, 2011.
- 10 Laske, G. and Masters, G.: A Global Digital Map of Sediment Thickness, *EOS Trans. AGU*, 78, 1997.
- Lynch-Stieglitz, J., Schmidt, M. W., Henry, L. G., Curry, W. B., Skinner, L. C., Mulitza, S., Zhang, R., and Chang, P.: Muted change in Atlantic overturning circulation over some glacial-aged Heinrich events, *Nature Geoscience*, 7, 144–150, <https://doi.org/10.1038/ngeo2045>, 2014.
- Lüthi, D., Floch, M. L., Bereiter, B., Blunier, T., Barnola, J.-M., Siegenthaler, U., Raynaud, D., Jouzel, J., Fischer, H., Kawamura, K., and Stocker, T. F.: High-resolution carbon dioxide concentration record 650,000–800,000 years before present, *Nature*, 453, 379–382, <https://doi.org/10.1038/nature06949>, 2008.
- 15 MacAyeal, D. R.: Binge/Purge Oscillations of the Laurentide Ice Sheet as a Cause of the North Atlantic’s Heinrich Events, *Paleoceanography*, 8, <https://doi.org/10.1029/93PA02200>, 1993.
- Maier-Reimer, E. and Mikolajewicz, U.: Experiments with an OGCM on the Cause of the Younger Dryas, in: *Oceanogr. 1988*, edited by Wooster, W. and Yáñez-Arancibia, UNAM Press, México D F, 1989.
- 20 Mikolajewicz, U., Gröger, M., Maier-Reimer, E., Schurgers, G., Vizcaíno, M., and Winguth, A. M. E.: Long-term effects of anthropogenic CO<sub>2</sub> emissions simulated with a complex earth system model, *Clim. Dyn.*, 28, 599–633, <https://doi.org/10.1007/s00382-006-0204-y>, <http://www.springerlink.com/index/10.1007/s00382-006-0204-y>, 2007a.
- Mikolajewicz, U., Vizcaíno, M., Jungclaus, J., and Schurgers, G.: Effect of ice sheet interactions in anthropogenic climate change simulations, *Geophys. Res. Lett.*, 34, <https://doi.org/10.1029/2007GL031173>, 2007b.
- 25 Moros, M., Kuijpers, A., Snowball, I., Lassen, S., Bäckström, D., Gingele, F., and McManus, J.: Were glacial iceberg surges in the North Atlantic triggered by climatic warming?, *Marine Geology*, 192, 393–417, [https://doi.org/10.1016/s0025-3227\(02\)00592-3](https://doi.org/10.1016/s0025-3227(02)00592-3), 2002.
- Otto-Bliesner, B. L. and Brady, E. C.: The sensitivity of the climate response to the magnitude and location of freshwater forcing: last glacial maximum experiments, *Quat. Sci. Rev.*, 29, 56–73, <https://doi.org/10.1016/j.quascirev.2009.07.004>, 2010.
- Peltier, W. R.: Global glacial isostasy and the surface of the ice-age earth: The ice-5G (VM2) model and grace, *Annu. Rev. Earth Planet. Sci.*, 32, 111–149, <https://doi.org/10.1146/annurev.earth.32.082503.144359>, <http://www.annualreviews.org/doi/abs/10.1146/annurev.earth.32.082503.144359>, 2004.
- 30 Roberts, W. H. G., Valdes, P. J., and Payne, A. J.: A new constraint on the size of Heinrich Events from an iceberg/sediment model, *Earth Planet. Sci. Lett.*, 386, 1–9, <https://doi.org/http://dx.doi.org/10.1016/j.epsl.2013.10.020>, <http://www.sciencedirect.com/science/article/pii/S0012821X13005839>, 2014a.
- 35 Roberts, W. H. G., Valdes, P. J., and Payne, A. J.: Topography’s crucial role in Heinrich Events, *Proc. Natl. Acad. Sci.*, 111, 16 688–16 693, <https://doi.org/10.1073/pnas.1414882111>, <http://www.pnas.org/lookup/doi/10.1073/pnas.1414882111>, 2014b.
- Roberts, W. H. G., Payne, A. J., and Valdes, P. J.: The role of basal hydrology in the surging of the Laurentide Ice Sheet, *Climate of the Past*, 12, 1601–1617, <https://doi.org/10.5194/cp-12-1601-2016>, 2016.



- Schiller, A., Mikolajewicz, U., and Voss, R.: The stability of the North Atlantic thermohaline circulation in a coupled ocean-atmosphere general circulation model, *Clim. Dyn.*, 13, 325–347, <http://dx.doi.org/10.1007/s003820050169>, 1997.
- Spahni, R. and Stocker, T. F.: EPICA Dome C atmospheric methane concentrations to 650 kyr BP, <https://doi.org/10.1594/PANGAEA.472484>, <https://doi.org/10.1594/PANGAEA.472484>, 2006a.
- 5 Spahni, R. and Stocker, T. F.: EPICA Dome C atmospheric nitrous oxide concentrations to 650 kyr BP, <https://doi.org/10.1594/PANGAEA.472487>, <https://doi.org/10.1594/PANGAEA.472487>, 2006b.
- Stanford, J. D., Rohling, E. J., Bacon, S., Roberts, A. P., Grousset, F. E., and Bolshaw, M.: A new concept for the paleoceanographic evolution of Heinrich event 1 in the North Atlantic, *Quat. Sci. Rev.*, 30, 1047–1066, <https://doi.org/10.1016/j.quascirev.2011.02.003>, 2011.
- Stokes, C. R. and Tarasov, L.: Ice streaming in the Laurentide Ice Sheet: A first comparison between data-calibrated numerical model output  
10 and geological evidence, *Geophys. Res. Lett.*, 37, <https://doi.org/10.1029/2009GL040990>, 2010.
- Stouffer, R. J., Yin, J., Gregory, J. M., Dixon, K. W., Spelman, M. J., Hurlin, W., Weaver, A. J., Eby, M., Flato, G. M., Hasumi, H., Hu, A., Jungclaus, J. H., Kamenkovich, I. V., Levermann, A., Montoya, M., Murakami, S., Nawrath, S., Oka, A., Peltier, W. R., Robitaille, D. Y., Sokolov, A., Vettoretti, G., and Weber, S. L.: Investigating the Causes of the Response of the Thermohaline Circulation to Past and Future Climate Changes, *J. Clim.*, 19, 1365–1387, <https://doi.org/10.1175/JCLI3689.1>, 2006.
- 15 Van Pelt, W. J. J. and Oerlemans, J.: Numerical simulations of cyclic behaviour in the Parallel Ice Sheet Model (PISM), *J. Glaciol.*, 58, 347–360, <https://doi.org/10.3189/2012JoG11J217>, 2012.
- Voss, R. and Sausen, R.: Techniques for asynchronous and periodically synchronous coupling of atmosphere and ocean models, *Climate Dynamics*, 12, 605–614, <https://doi.org/10.1007/bf00216269>, 1996.
- Winkelmann, R., Martin, M. A., Haseloff, M., Albrecht, T., Bueler, E., Khroulev, C., and Levermann, A.: The Potsdam Parallel Ice Sheet  
20 Model (PISM-PIK) Part 1: Model description, *Cryosph.*, 5, 715–726, <https://doi.org/10.5194/tc-5-715-2011>, 2011.
- Ziemen, F. A., Rodehacke, C. B., and Mikolajewicz, U.: Coupled ice sheet–climate modeling under glacial and pre-industrial boundary conditions, *Clim. Past*, 10, 1817–1836, <https://doi.org/10.5194/cp-10-1817-2014>, <http://www.clim-past.net/10/1817/2014/>, 2014.

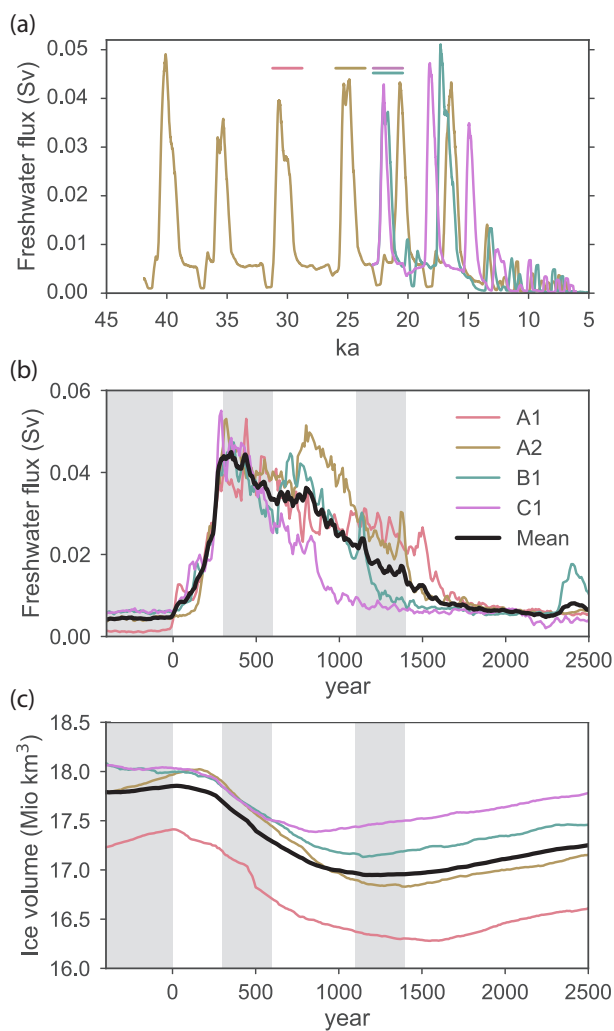


**Figure 1.** (a), (b) Hudson Strait Ice Stream discharge, (c) Ice volume of the eastern Part of the Laurentide Ice Sheet. (a) is averaged over 300 years, (b) over 30 years, (c) is plotted from instantaneous values. Line colors in (a) correspond to Heinrich events A2, B1, and C1, horizontal bars mark the events selected for the composite analysis in the colors used throughout the time series analysis. The vertical gray bars in (b,c) mark the pre-surge (years  $-400$  to  $0$ ), surge (years  $300$  to  $600$ ), and post-surge (years  $1100$  to  $1400$ ) phases (Section 2.3).  $1 \text{ Mio km}^3$  of ice corresponds to about  $2.5 \text{ m}$  of sea level.

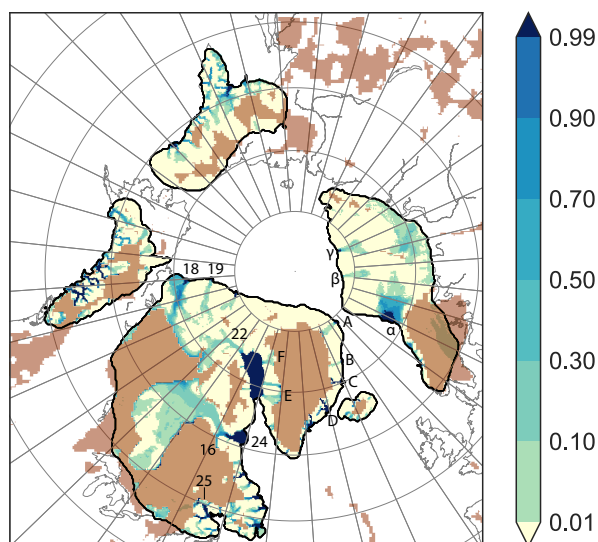


**Figure 2.** Colors from the color bar mark the fraction of time that a grid cell in the glacial part of ExA (41 ka–15.6 ka) is sliding or has floating ice with a basal velocity exceeding  $1 \text{ m yr}^{-1}$ . Only the time when the grid cell is ice covered is taken into consideration; therefore, ice shelves are considered to be constantly sliding. Only areas with a time-mean ice thickness in excess of 10 m are displayed. Brown marks areas where the ice is not permitted to slide due to the lack of sediments in the reconstruction of Laske and Masters (1997). Numbers match the ice stream numbering in Stokes and Tarasov (2010), and are as follows: (16) Ungava Bay, (18) Amundsen Gulf, (19) M’Clure Strait, (22) Lancaster Sound, (24) Hudson Strait, (25) Laurentian. Letters refer to present-day location names of modeled Greenland ice streams: (A) Northeast Greenland Ice Stream, (B) Kejsler Franz Joseph Fjord, (C) Scoresby Sund, (D) Kangerdlugssuaq, (E) Jakobshavn Isbrae, (F) Kong Oscar Glacier. Greek letters ( $\alpha, \beta, \gamma$ ) mark Barents Shelf ice streams. In the Baltic Sea, the ice sheet retreats at the start of the experiment, so there temporarily is an ice shelf.

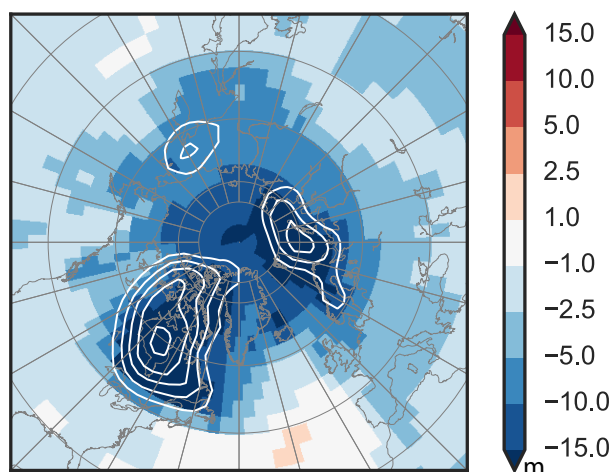


**Figure 3.** Temperature difference pre-surge phase – pre-industrial experiment, overlay: topography increase from pre-industrial to pre-surge glacial state (mostly ice sheets) as seen by ECHAM5 at multiples of 500 m. For a definition of the pre-surge phase see Fig. 1 and Section 2.3.

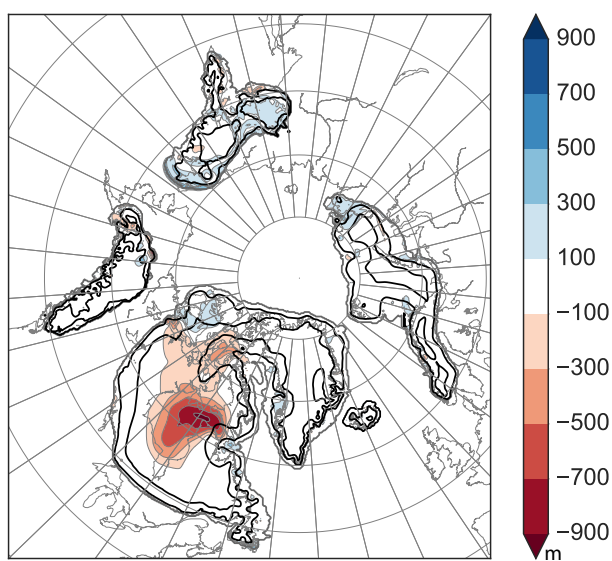


**Figure 4.** Ice surface elevation change in composite year 1250 compared with composite year  $-50$ . Overlays mark ice sheet outline (gray) and surface elevation (black) at 1000, 2000, 3000 m in the pre-surge phase. The Laurentide ice sheet barely misses 3000 m. The peak of Greenland slightly exceeds this elevation.

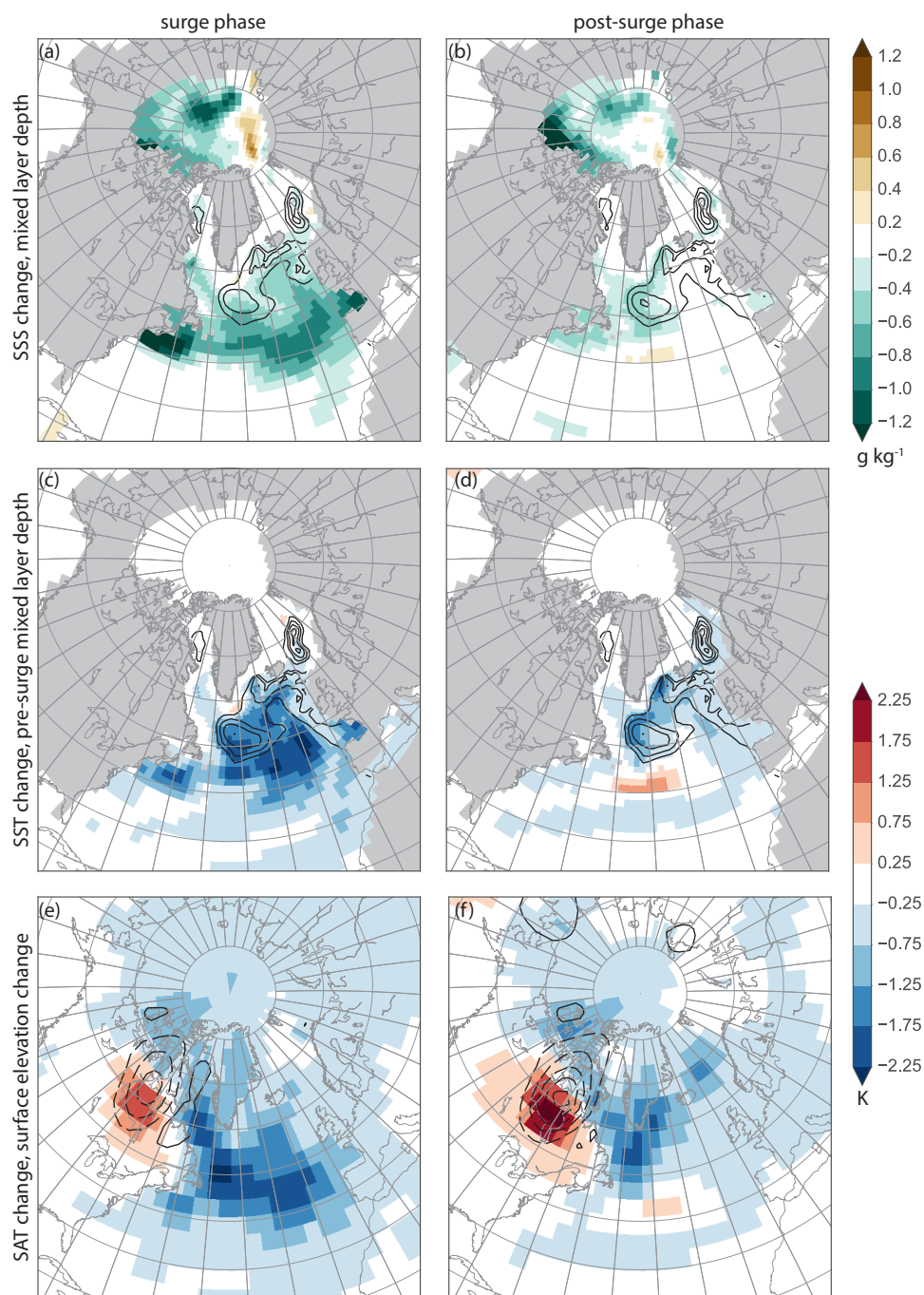


**Figure 5.** (a,b) Sea surface salinity, (c,d) sea surface temperature, and (e,f) surface air temperature changes compared to the pre-surge state during (a,c,e) the surge phase and (b,d,f) the post-surge phase. The overlays show (a,b) maximum mixed layered depth during the respective phases of the event at multiples of 500 m (maximum of the 300-year climatology), (c,d) maximum mixed layer depth in the pre-surge phase (same scale), and (e,f) elevation changes in the respective phases of the event vs. the pre-surge phase (at multiples of 100 m, dashed lines mark negative values, solid lines positive values). For a definition of the phases see Fig. 1 and Section 2.3.

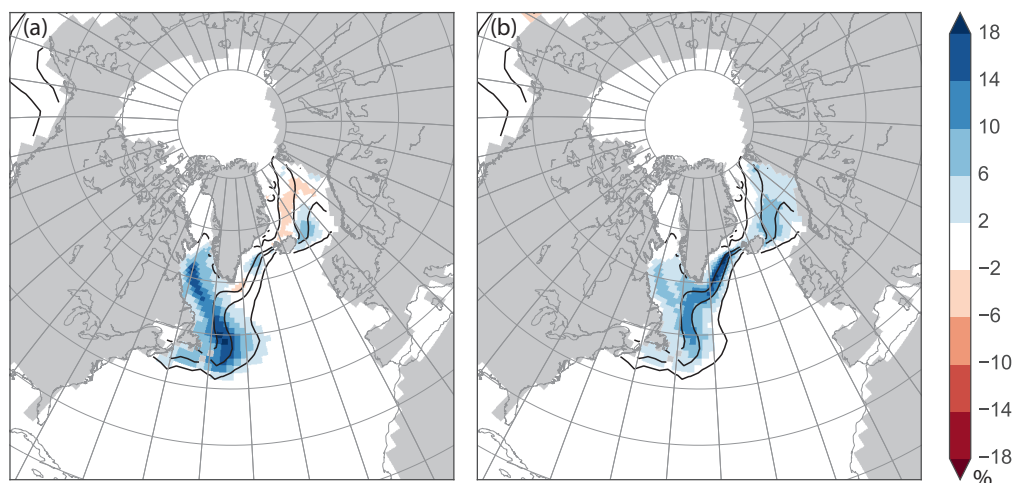


**Figure 6.** Sea-ice concentration change compared to the pre-surge phase for (a) surge phase, and (b) post-surge phase. Overlays mark sea-ice concentration in the pre-surge phase on levels of 1, 15, 50, and 95%. For a definition of the phases see Fig. 1 and Section 2.3.

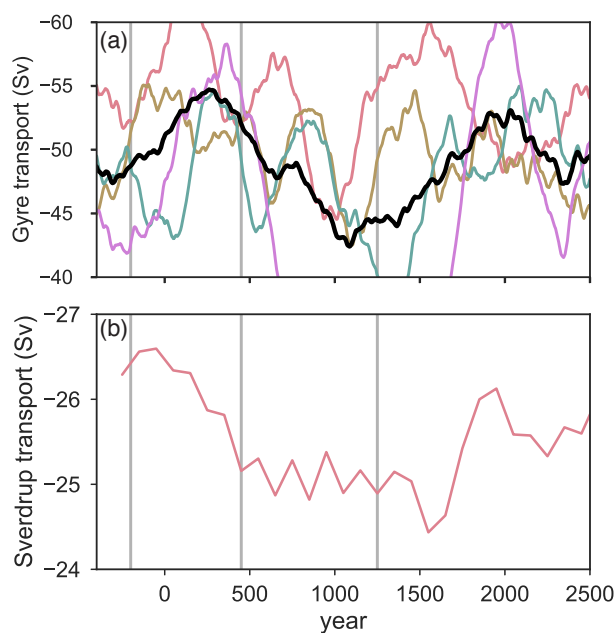


**Figure 7.** Strength of the North Atlantic subpolar gyre and the windstress contribution (Sverdrup transport). (a) 300 year running mean, (b) 300 year block means. Colors as in Fig. 1. Vertical lines mark the centers of the intervals selected for the analysis. As this figure is using 300 year averaging, they indicate the average values corresponding to the time windows used in the analysis. Note the different scales for gyre and Sverdrup transport.

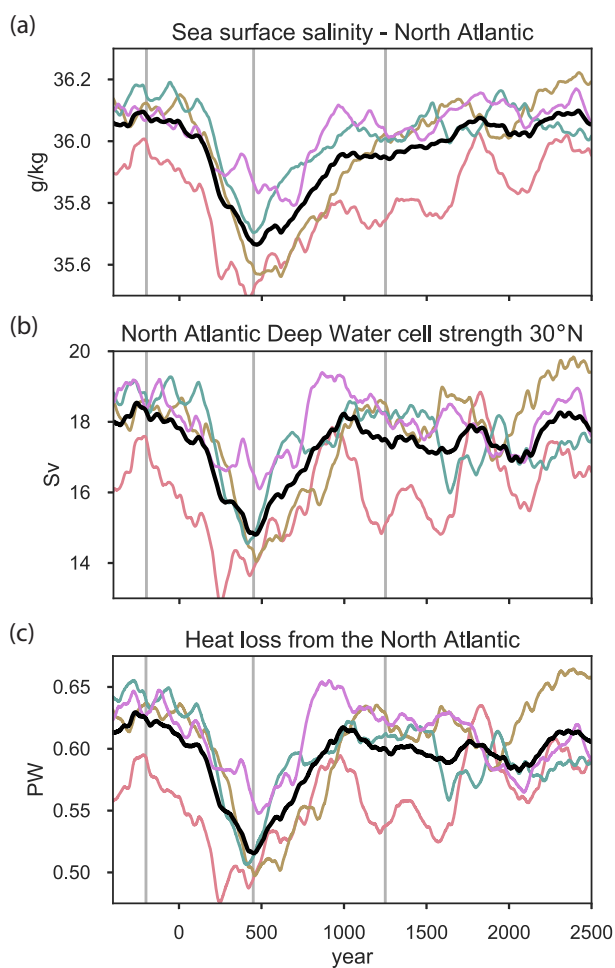


**Figure 8.** (a) North Atlantic Sea surface salinity, (b) NADW cell strength at 30°N and (c) North Atlantic Heat loss. 300 year running means. Colors as in Fig. 1, vertical lines as in Fig. 7.

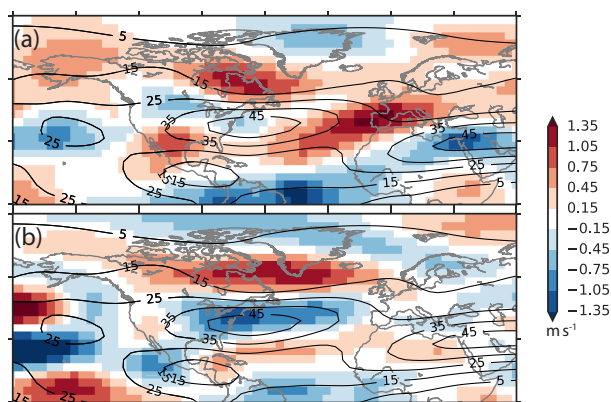


**Figure 9.** DJF 200 hPa zonal wind speed anomalies compared to the pre-surge phase. Overlays show zonal wind speeds in the pre-surge phase in  $\text{ms}^{-1}$ . Dashed lines mark negative values. (a) surge phase, (b) post-surge phase. Note the projection with focus on the North Atlantic. For a definition of the phases see Fig. 1 and Section 2.3.

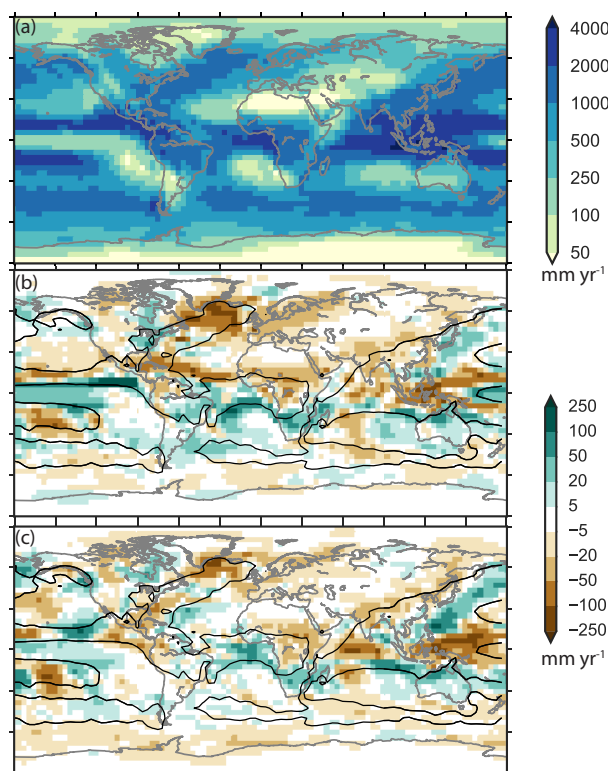


**Figure 10.** (a) annual mean precipitation in the pre-surge phase, (b,c) precipitation changes in (b) the surge phase and (c) the post-surge phase with pre-surge  $1 \text{ mm yr}^{-1}$  isoline overlain to allow for an easier identification of the ITCZ. For a definition of the phases see Fig. 1 and Section 2.3.

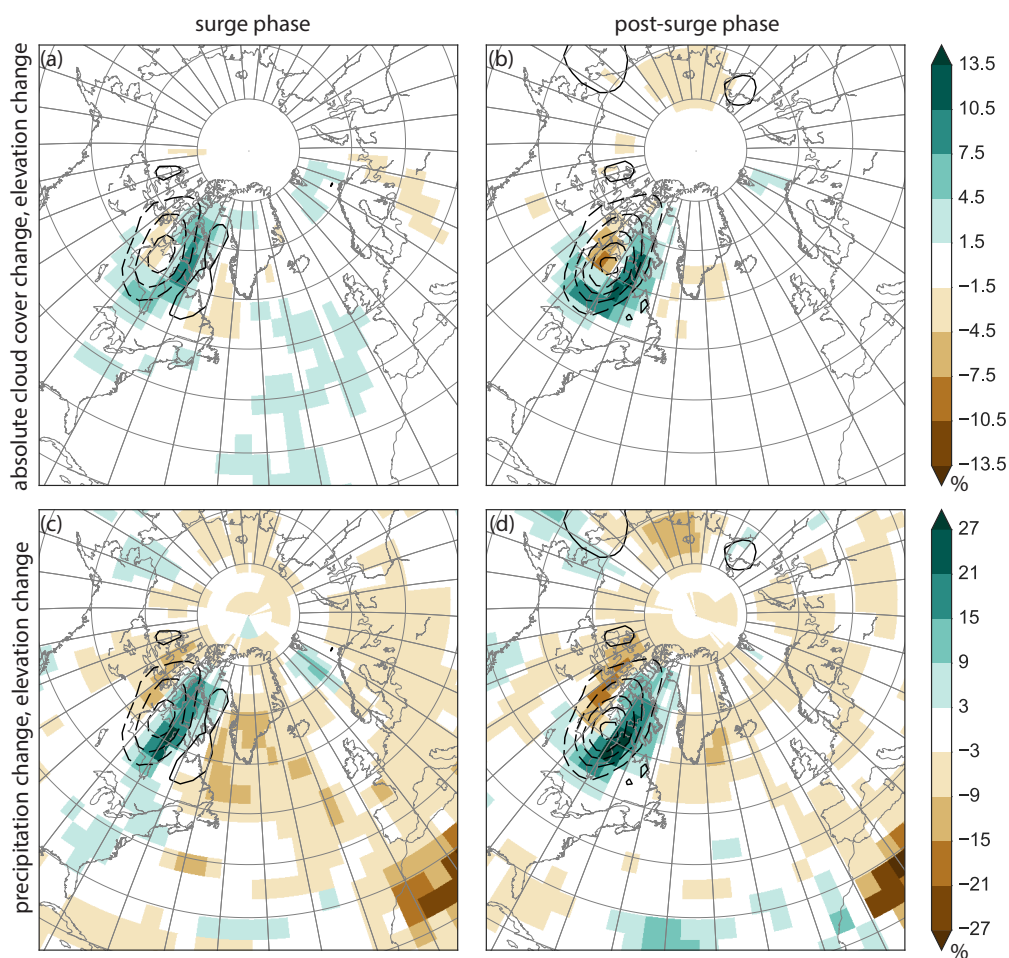


**Figure 11.** (a,b) Total cloud cover changes, and (c,d) relative changes in precipitation. (a,c) surge phase, (b,d) post-surge phase. Isolines mark the ice sheet elevation change at multiples of 100 m. Dashed lines mark negative values. All changes are relative to the pre-surge phase. For a definition of the phases see Fig. 1 and Section 2.3.